Stratigraphy and shale geochemistry of the Belcher Group, Belcher Islands, southern Nunavut

M.S.W. Hodgskiss[1] and E.A. Sperling[2]

[1]*Department of Geological Sciences, Stanford University, Stanford, California, United States, mswh@stanford.edu*
[2]*Department of Geological Sciences, Stanford University, Stanford, California, United States*

Hodgskiss, M.S.W. and Sperling, E.A. 2020: Stratigraphy and shale geochemistry of the Belcher Group, Belcher Islands, southern Nunavut; *in* Summary of Activities 2019, Canada-Nunavut Geoscience Office, p. 65–78.

Abstract

The Belcher Group contains what is arguably the best-preserved and most spectacular geological record of the Orosirian period (2.05–1.8 Ga) in northern Canada and perhaps the world. Recent studies have made significant progress toward understanding this succession using carbon and oxygen isotope chemostratigraphy of carbonate sedimentary rocks, U-Pb zircon geochronology and triple-oxygen isotope analyses of barite crystals, although the shale geochemistry of the succession has been largely overlooked. Here, new iron speciation data are presented that show deposition of shale units within the Costello Formation took place within ferruginous waters, whereas the Laddie Formation was deposited within a weakly oxic to ferruginous water column and represents a potential marine redbed. Shale interbedded with pillow basalt of the Flaherty Formation likely records deposition within euxinic waters—the only such occurrence within the Belcher Group. Overall, these data point toward a depositional environment of weakly oxic surface waters with an intermittently deep oxycline.

Résumé

Le Groupe de Belcher renferme ce qui sont potentiellement les témoins géologiques les mieux préservés et les plus spectaculaires de la période de l'Orosirien (2,05–1,8 Ga) du nord du Canada, sinon du monde. De récents travaux ont permis aux chercheurs de réaliser des progrès considérables dans l'amélioration de leur compréhension de cette succession en ayant recours à la chimiostratigraphie isotopique (carbone et oxygène) des roches sédimentaires carbonatées, de la datation par la méthode U-Pb sur zircon et de l'analyse des isotopes stables de l'oxygène (^{16}O, ^{17}O, ^{18}O) dans la barytine, bien que la géochimie des schistes argileux de la succession ait été en grande partie négligée. Le présent article fait état de nouvelles données relatives à la spéciation du fer qui démontrent que la mise en place des unités schisteuses au sein de la Formation de Costello aurait eu lieu dans des eaux ferrugineuses, alors que la Formation de Laddie aurait été mise en place dans une colonne d'eau faiblement oxydante à ferrugineuse, de façon à ce qu'elle puisse être considérée une couche rouge marine. Du schiste argileux intercalé avec du basalte en coussins de la Formation de Flaherty témoigne de sédimentation qui se serait produite dans un milieu euxinique, soit l'unique manifestation de ce phénomène au sein du Groupe de Belcher. En général, les données semblent indiquer qu'il s'agissait d'un milieu sédimentaire à eaux de surface faiblement oxydantes caractérisé par la présence d'une oxycline occasionnellement profonde.

Introduction

The Belcher Group is a mixed carbonate-clastic-volcanic succession exposed in the Belcher Islands, in Hudson Bay, southern Nunavut, near the northern margin of the Superior craton. It is coeval with a series of mid-Paleoproterozoic packages circumferencing nearly the entirety of the craton (clockwise they are the Belcher Group, Cape Smith Belt, Labrador Trough, Mistassini and Otish groups, Lake Superior association, Fox River Belt and Sutton Inlier; Baragar and Scoates, 1981). The geology of this remote archipelago (Figure 1) has been studied intermittently since the early 1900s, and most intensely during the 1950s–1970s (e.g., Moore, 1918; Jackson, 1960, 1961; Dimroth et al., 1970; Ricketts, 1979; reviewed by Jackson, 2013), resulting in the construction of a robust geological framework for the region. Recent efforts led by the first author resulted in high-resolution $\delta^{13}C$ and $\delta^{18}O$ chemostratigraphic curves through the succession, several new U-Pb zircon depositional ages (Hodgskiss et al., 2019b) and triple oxygen iso-

This publication is also available, free of charge, as colour digital files in Adobe Acrobat® PDF format from the Canada-Nunavut Geoscience Office website: http://cngo.ca/summary-of-activities/2019/.

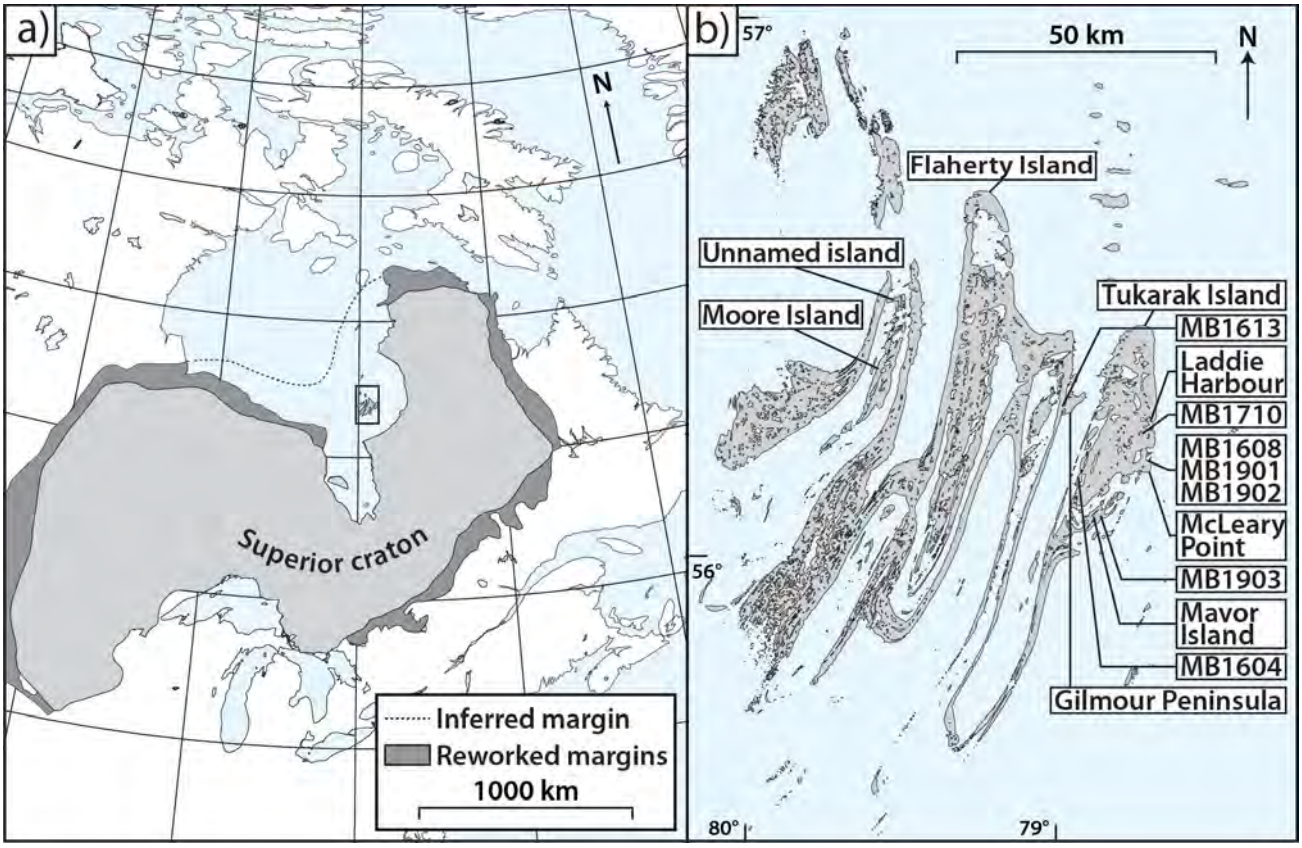

Figure 1: a) The Belcher Islands (in black box) shown relative to the Superior craton. **b)** Shale sampling sites; labels correspond to stratigraphic sections. Modified from Hodgskiss et al. (2019b).

tope measurements of barite crystals (Hodgskiss et al., 2019a). Shale geochemistry, which has not previously been analyzed in the Belcher Group, has the potential to constrain different aspects of the depositional system than those typically ascertained by carbonate geochemistry analyses, especially with regards to understanding the redox conditions in which sediments were deposited. In this study, iron speciation (the partitioning of iron between different operational mineral pools) is used to determine if shale units were deposited in oxic, ferruginous (containing excess ferrous iron) or euxinic (containing excess free sulphide) conditions. Constraining the redox chemistry of sedimentary deposits is important for understanding how ocean and atmosphere chemistry has changed through the Earth's history, and how it may have impacted the evolution of life. Redox conditions are also important for understanding the formation of sedimentary mineral deposits. These analyses were coupled with the first drone imagery of the Belcher Group, which is useful for visualizing these formations against the extremely low topographic relief of the archipelago.

Stratigraphy

The Belcher Group was informally divided into six depositional phases by Ricketts (1979) and Ricketts and Donaldson (1981). Contacts between formations are conformable, and vary from sharp to gradational over several metres; no significant erosional unconformities have been observed in the Belcher Group. Although the basement rocks underlying the Belcher Group are not exposed, it is thought to lie on top of crystalline rocks of the Superior craton (supported by detrital zircon analyses; Hodgskiss et al., 2019b). Deposition of the Belcher Group initiated with the development of a transgressive carbonate platform represented by the Kasegalik Formation, an approximately 1.1 km thick succession of supratidal to intertidal dolomicrite and argillaceous dolomicrite (Figures 2, 3a). Subordinate sandstone interbeds exhibit herringbone crossbedding. Stromatolites and bioherms occur through the formation, some with evidence for chemical precipitation of aragonite needles (Hofmann and Jackson, 1987). Gypsum pseudomorphs are abundant, with halite casts occurring less frequently. Tuff beds ~1 m thick were reported by Dimroth et al. (1970), with additional centimetre-thick tuffs identified and detailed by Hodgskiss et al. (2019b). Overall, the Kasegalik Formation has been interpreted as representing a gentle deepening-upward sequence from sabkha to shallow subtidal conditions (Ricketts, 1979). The U-Pb analyses of zircons from tuffs in the lower and upper Kasegalik Formation constrain its deposition to between 2018.5 ±1.0 and 2015.4 ±1.8 Ma (Hodgskiss et al., 2019b). The accumulation of ~1 km of sedimentary rock in just

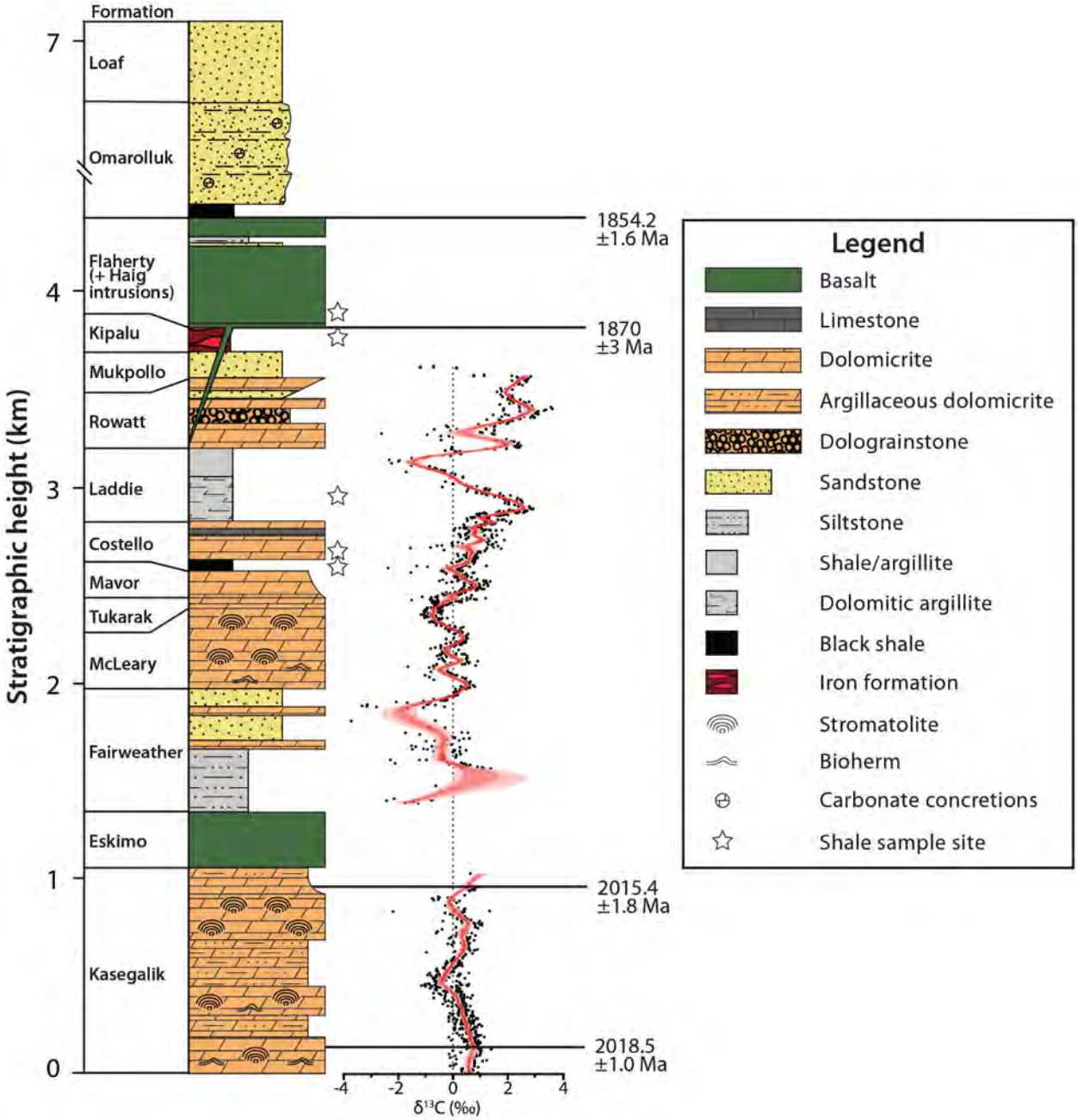

Figure 2: Schematic stratigraphic section of the Belcher Group, Belcher Islands, with age constraints and $\delta^{13}C$ data from Hodgskiss et al. (2019b) and Hamilton et al. (2009). Note the break in scale between 4 and 7 km. Modified from Hodgskiss et al. (2019a).

3 m.y. led Hodgskiss et al. (2019b) to suggest that deposition of the Kasegalik Formation occurred during initial rifting of the basin. Although this package lacks the typical characteristics of a rift sequence (e.g., immature clastic sediments), the lower contact with the crystalline basement is not exposed.

The next depositional phase is characterized largely by massive, aphanitic, green-grey basalt flows of the Eskimo Formation (200 to 1000 m thick; Figures 2, 3a). Columnar jointing is common, and pillow basalts are rare. Red, thinly bedded siltstone, sandstone and conglomerate units up to several metres thick occur (Jackson, 2013). An ~30 cm thick interbed of granular iron formation is exposed within the basalt on the eastern side of an unnamed island in northern Churchill Sound (the same unnamed island in Hofmann, 1976; Figure 1b). Overall, the Eskimo Formation is interpreted to represent dominantly subaerial volcanism with occasional fluvial deposition, represented by clastic sedimentary rocks.

The flood basalt phase was followed by deposition of a second transgressive carbonate platform beginning with shallow marine sandstone and siltstone with minor carbonate

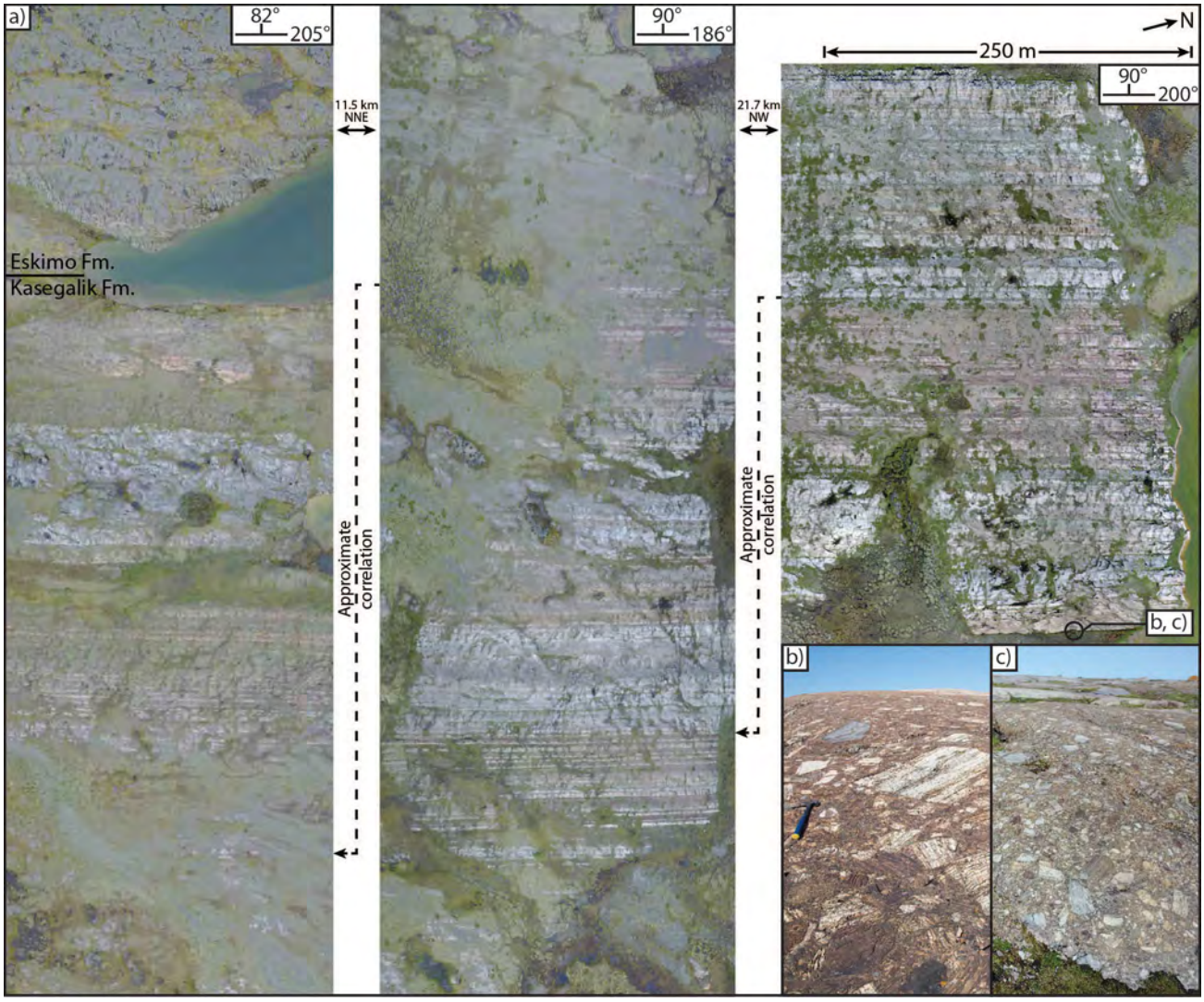

Figure 3: The Kasegalik Formation in the Belcher Islands. **a)** Drone photomosaics from Moore Island (left image), central Flaherty Island (central image) and southern Flaherty Island (right image) provide a near-complete composite 'section' of the Kasegalik Formation. The most prominent features are red-pink interbedded dolomicrite, argillaceous dolomicrite, and thick grey dolomicrite units. Bedding symbol indicates strike and dip. **b, c)** Breccia at the base of a section on Moore Island, likely from folding and associated faulting. Clasts reach up to 1 m in width. Abbreviations: NNE, north-northeast; NW, northwest.

lithologies (e.g., pisoids, dolomicrite, stromatolites) of the Fairweather Formation (350 to 600 m thick; Figures 2, 4a). The overlying McLeary Formation (250 to 470 m thick; Figures 2, 4a) is composed of dolomicrite, sandstone and sandy dolomicrite. Black chert nodules and horizons are abundant in the upper portion of the formation, which is also notable for its remarkably diverse stromatolite morphologies. Desiccation cracks and very rare gypsum pseudomorphs have been observed (Bell and Jackson, 1974; Hodgskiss et al., 2019a). The Tukarak Formation (50 to 90 m thick) is largely composed of very thinly interbedded argillaceous maroon dolomicrite and grey-pink calcite. Beach stone rosettes composed of locally derived calcite clasts are common. The Mavor Formation (190 to 250 m thick; Figures 2, 4a) is composed primarily of dolomicrite and stromatolitic dolostone. On eastern Tukarak Island, these stromatolites form an impressive 'spur and groove' reef system some 200 m thick (Figure 4b; Ricketts and Donaldson, 1988). The Costello Formation (240 to 370 m thick; Figures 2, 4b, 5a) consists of 20 to 40 m of grey to black shale (generally not exposed), overlain by hundreds of metres of very thinly interbedded dolomicrite and calcite in approximately equal proportions. Slump folds, very thin shale interbeds, grading and partial Bouma sequences have led to the interpretation that these sediments were deposited in deep waters with turbidite activity (Ricketts, 1979). The uppermost formation in this package is the Laddie Formation (~230 m; Figure 2), largely composed of brick red shale with a minor carbonate component in the matrix, as well as laminae, very thin beds and nodules of white-pink

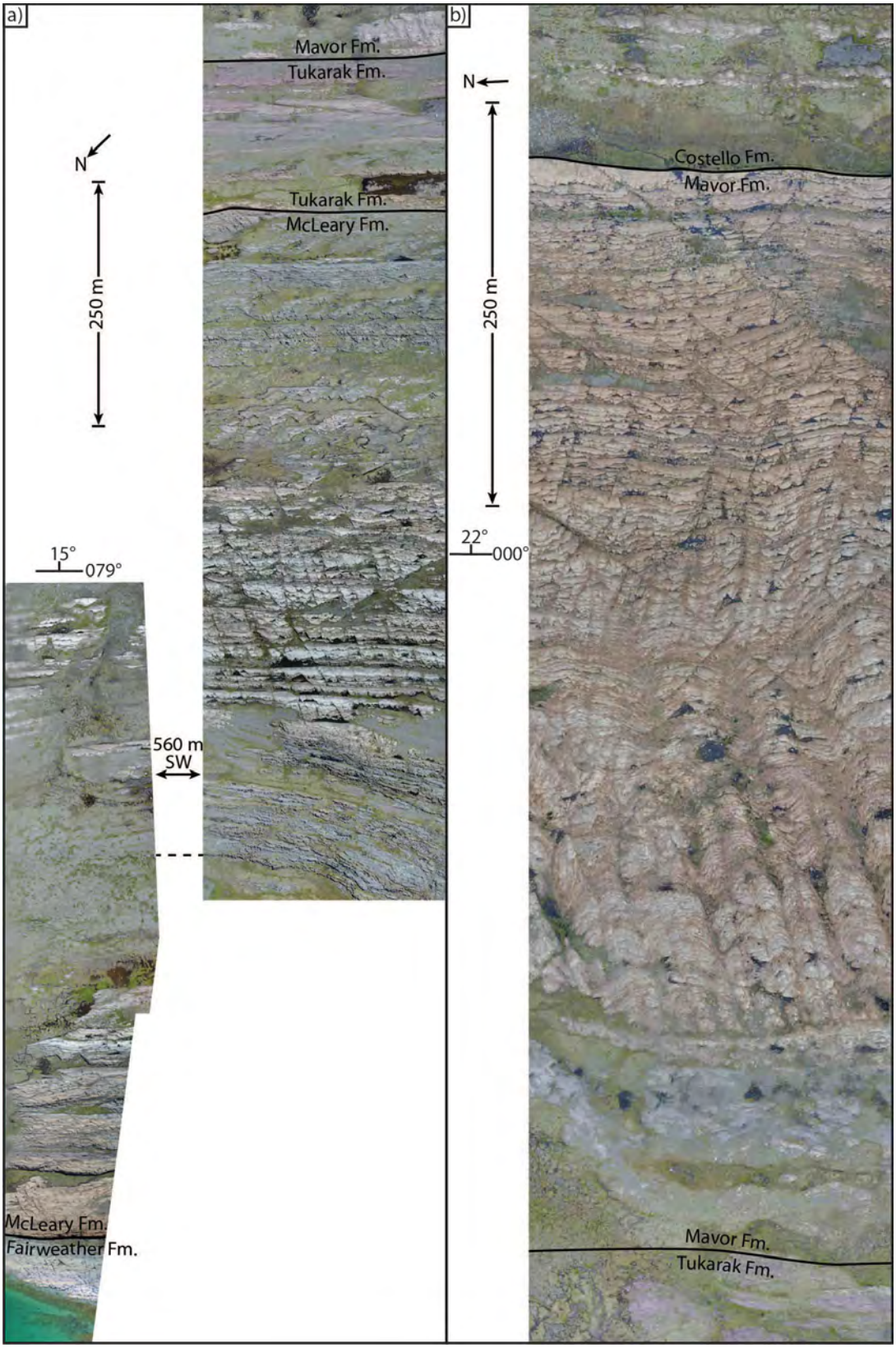

Figure 4: a) Drone photomosaic of the uppermost Fairweather Formation through lower Mavor Formation on western Mavor Island. **b)** Drone photomosaic of the Mavor Formation stromatolite reef complex on eastern Tukarak Island. Bedding symbol indicates strike and dip. Abbreviation: SW, southwest.

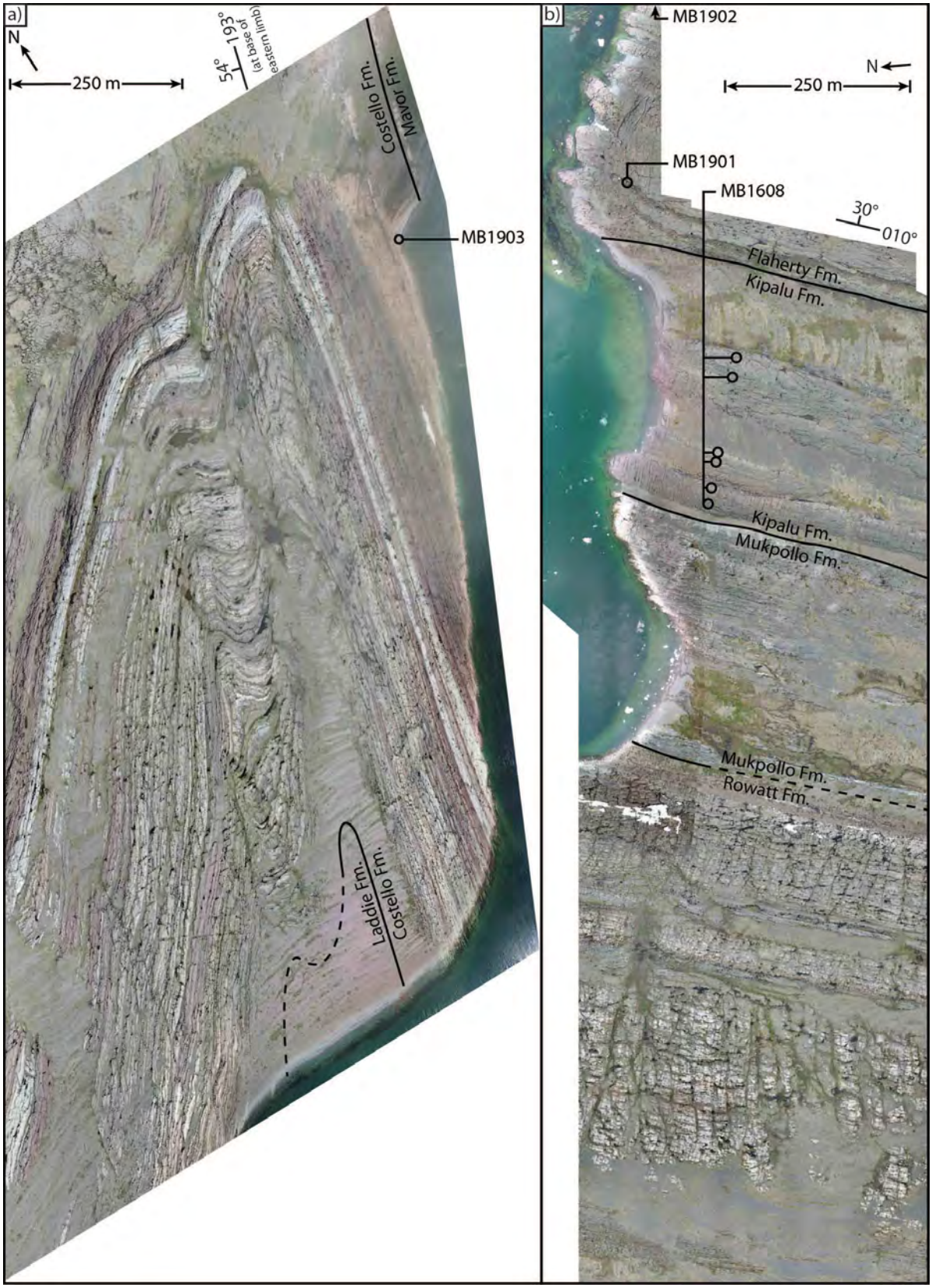

Figure 5: a) Drone photomosaic of the uppermost Mavor Formation through lowermost Laddie Formation on southeastern Mavor Island. Sampling location of section MB1903 indicated by black circle. **b)** Drone photomosaic of the upper Rowatt Formation through lower Flaherty Formation on the southern side of an unnamed bay, north of McLeary Point on Tukarak Island. Sampling locations for sections MB1608, MB1901 and MB1902 indicated by black circles and arrow. Bedding symbol indicates strike and dip.

calcite and dolomicrite. The upper portion of the formation is composed of siltstone and crossbedded sandstone. The Laddie Formation is interpreted to have been deposited in a deep basin below storm-wave base (Ricketts, 1979; Ricketts and Donaldson, 1988).

The next depositional phase begins with the Rowatt Formation (330 m thick; Figures 2, 5b), which grades from siltstone and sandstone with abundant crossbedding (including herringbone and reactivation surfaces) to dolograinstone and dolomicrite with extreme soft-sediment deformation and minor channelization. The Rowatt Formation represents progradation and potentially the development of a restricted basin. The overlying Mukpollo Formation (120 to 160 m thick; Figures 2, 5b) is composed almost entirely of quartz sandstone, with minor siltstone and dolomitic quartz sandstone. Herringbone crossbedding, desiccation cracks and channelization (with lag) indicate deposition in a tidal-influenced environment with intermittent subaerial exposure. The Kipalu Formation (80 to 130 m thick; Figures 2, 5b) is dominated by variably iron-rich argillite and lenses and nodular horizons of granular jasper (i.e., granular iron formation) with minor carbonate lithologies. These formations have been interpreted to record significant shallowing, from the deep starved basin of the preceding phase (Laddie Formation) to supratidal and intertidal carbonate rocks (Rowatt Formation) to intertidal, mature quartz sandstone (Mukpollo Formation) and, finally, argillite and granular iron formation representing a barred basin (Kipalu Formation; Ricketts, 1979). Although Ricketts (1979) interpreted deposition of the Kipalu Formation to have taken place under restricted basin conditions, the occurrence of numerous contemporary iron formations (e.g., Rasmussen et al., 2012) suggests that restriction may have been minor.

The following submarine volcanism phase is associated with the emplacement of significant mafic volcanic rocks. Composed solely of the Flaherty Formation (and associated Haig feeder dykes and sills; Dimroth et al., 1970; Figures 2, 5b), this phase is characterized primarily by pillow, columnar-jointed and massive basalt, totalling some 500 to 1600 m thick. Minor turbidite units are interbedded with basalt. The U-Pb analyses of baddeleyite from Haig dykes provide an age of 1870 ±3 Ma (Hamilton et al., 2009).

The final phase consists of a prograding submarine fan (Omarolluk Formation) and distal molasse (Loaf Formation). The Omarolluk Formation (at least 2100 m thick; Figure 2) is composed of shale, wacke, and sandstone with minor carbonate concretions, interpreted as a thick turbidite sequence (Ricketts, 1979). Analyses of zircons from a tuffaceous shale approximately 5 m above the Flaherty Formation–Omarolluk Formation contact provide an age of 1854.2 ±1.6 Ma (Hodgskiss et al., 2019b). Deposition of the Belcher Group concludes with the Loaf Formation (at least 620 m thick; Figure 2), which consists largely of extensively crossbedded sandstone with mud chips and intraformational conglomerate. Spectacular synsedimentary recumbent folding of crossbeds occurs in places, suggesting high sedimentation rates. Cumulatively, these lithologies and sedimentary structures have been used to interpret deposition in a braided river (Ricketts and Donaldson, 1981). Any stratigraphy that was originally overlying the Loaf Formation has been eroded over the ensuing ~1.8 b.y.

Sampling locations

Over the course of measuring stratigraphic sections through the Belcher Group, shale samples were collected from the rare fine-grained clastic units. In the lower Costello Formation near the abandoned Hudson's Bay Company outpost on western Tukarak Island, eight samples of black shale were collected from the siltstone-shale unit of the basal Costello Formation (section MB1604; Figure 6a). On southeastern Mavor Island, 11 samples from thin beds of dark grey shale interbedded with dolomicrite of the lower Costello Formation were collected (section MB1903; Figure 6b, c), approximately 35 m stratigraphically higher than the samples from MB1604. On eastern Tukarak Island, 16 samples of brick red and variably carbonate-rich shale of the lower Laddie Formation were collected (section MB1710; Figure 6d, e). Eight samples of variably iron-rich argillite from the Kipalu Formation were collected on southeastern Tukarak Island (section MB1608; Figure 6f). Finally, a total of 18 dark grey to black shale samples interbedded with basalt were collected from three locations on southeastern Tukarak Island and Gilmour Peninsula on eastern Flaherty Island (sections MB1901, MB1902, MB1613; Figure 7).

Methods

Iron speciation measurements were carried out at Stanford University (Stanford, California) using the sequential extraction protocol of Poulton and Canfield (2005), where iron is leached using acetate, dithionite and oxalate solutions. These leachates target iron in carbonates, oxides and magnetite, respectively, although the extractions are operational rather than truly mineral specific (especially the oxalate extraction; Slotznick et al., 2018b). Concentrations were measured following the ferrozine method of Stookey (1970) using a Thermo Scientific GENESYS™ 10S UV-Vis spectrophotometer, and the iron in pyrite was determined gravimetrically following a chromium reduction to extract sulphur (Canfield et al., 1986). Total iron was determined using a Bruker Tracer IV-SD handheld X-ray fluorescence spectrometer, with measurements recalibrated and drift-corrected using the United States Geological Survey SBC-1 standard reference material and internal standards. A subset of samples was analyzed for total organic

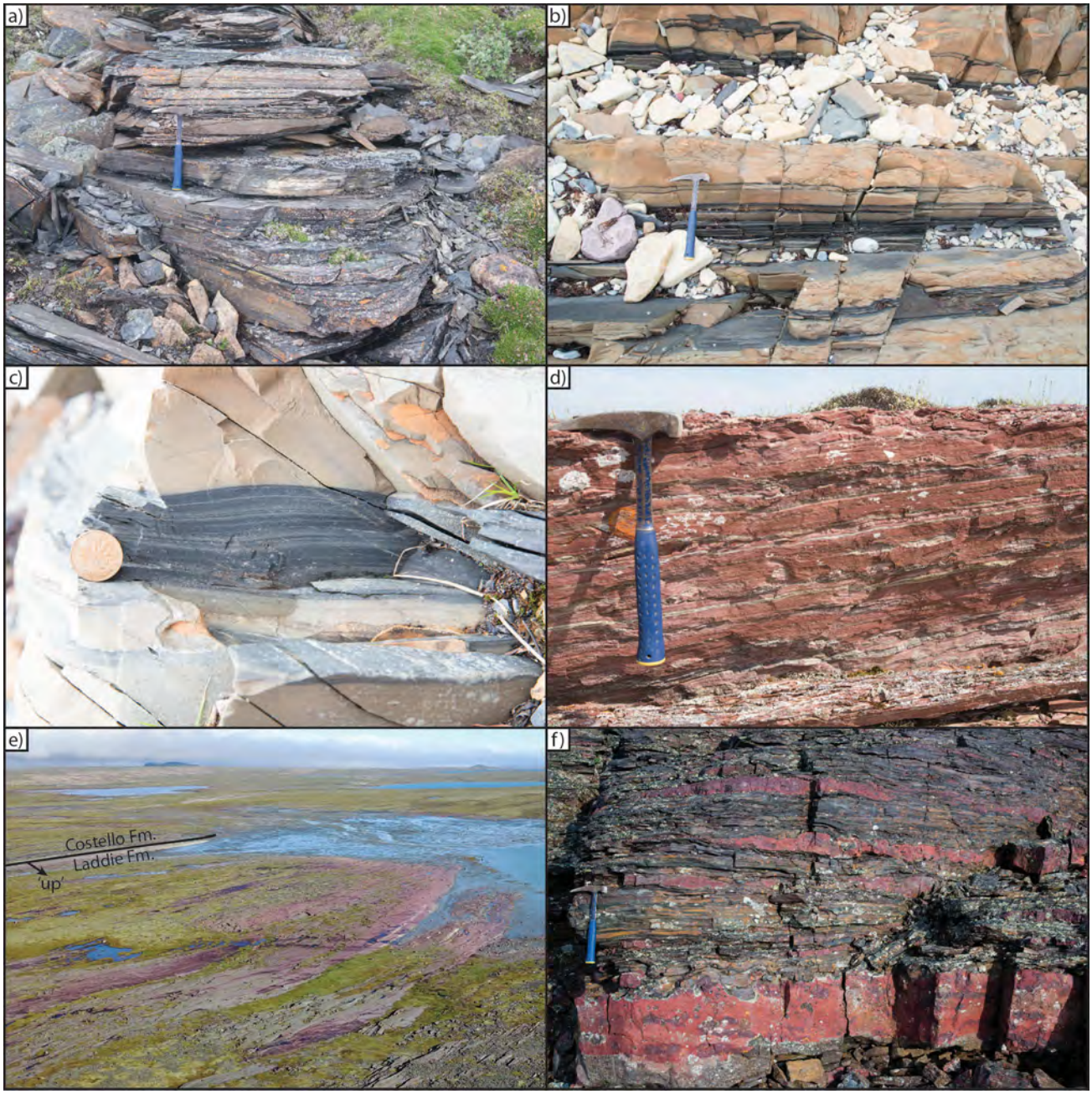

Figure 6: a) Shale outcrop of the Costello Formation sampled south of the abandoned Hudson's Bay Company outpost on western Tukarak Island (section MB1604). **b)** Thinly interbedded shale of the Costello Formation sampled on southeastern Mavor Island (section MB1903). **c)** Laminations visible in shale interbeds of the Costello Formation (section MB1903). **d)** The red Laddie Formation with laminations and nodules of carbonate (section MB1710). **e)** Drone photograph of the distinctly red Laddie Formation at southwestern Laddie Harbour, eastern Tukarak Island. Field of view is approximately 600 m across at the middle ground. **f)** Variably iron-rich argillite, and nodular horizons and lenses of granular iron formation of the Kipalu Formation (section MB1608).

carbon (TOC) contents using a Carlo Erba elemental analyzer. Prior to analyses, samples were decarbonated using 3*N* (Normal) HCl and rinsed thrice with deionized water. Drone imagery was captured using a DJI Mavic Pro, with imagery processed using Automotive Data Research's Maps Made Easy software, allowing for better contextualization of sampling within a stratigraphic section. Altitude (i.e., resolution) and camera settings were changed depending on weather conditions, topography, etc.

Results

Iron speciation results are discussed using six operationally defined iron pools: iron in carbonates (Fe_{carb}), oxides (Fe_{ox}), magnetite (Fe_{mag}) and pyrite (Fe_{py}), as well as iron that is unreactive (Fe_{un}) to the leaching methods described above, and total iron (Fe_T; Poulton and Canfield, 2005). Iron in carbonates, oxides, magnetite and pyrite combined represent 'highly reactive' iron (Fe_{HR}). In the canonical in-

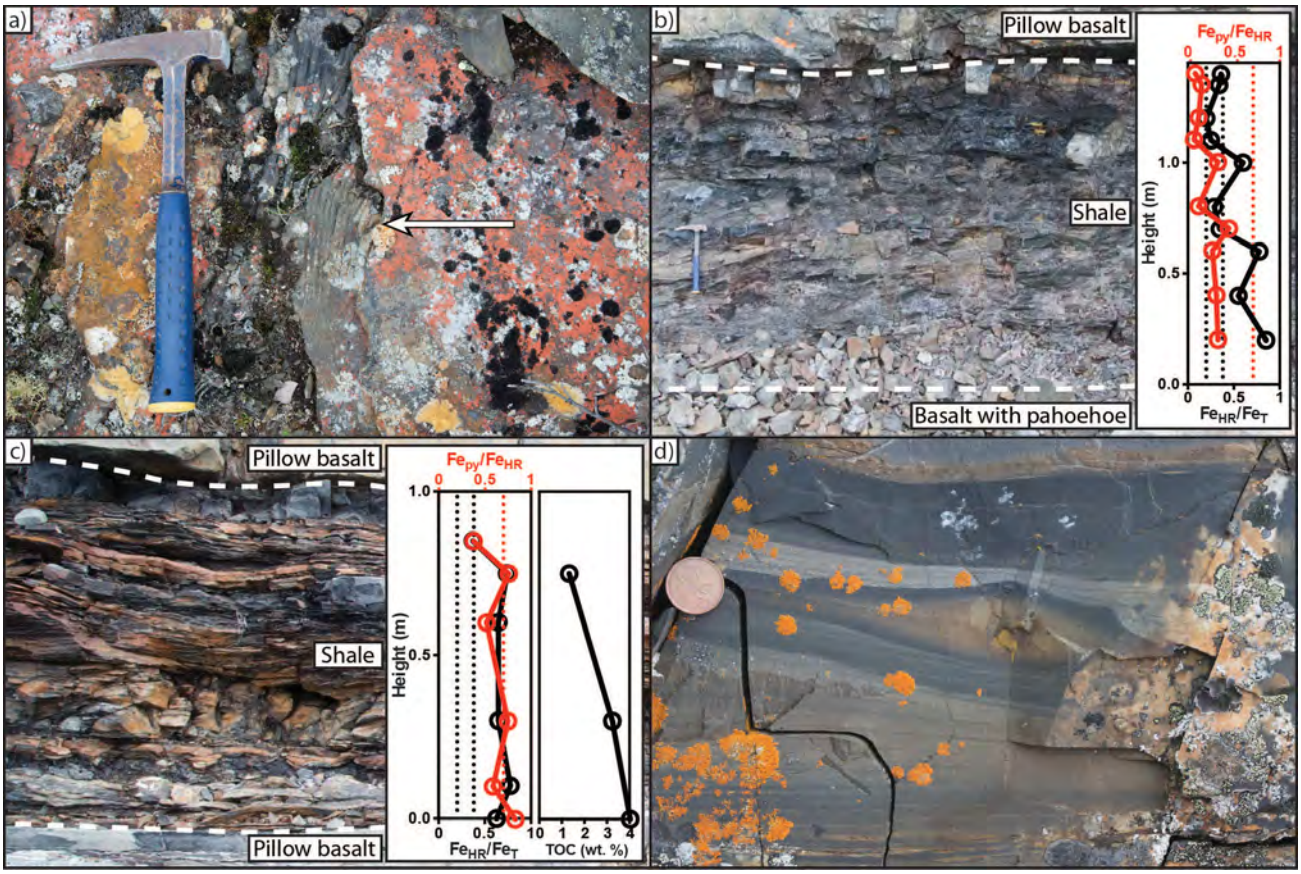

Figure 7: The Flaherty Formation, Belcher Islands. **a)** Basalt with pahoehoe texture (arrow) directly underlying the shale unit shown in b). **b)** An approximately 1.5 m thick shale unit directly overlies basalt with pahoehoe and underlies pillow basalt (section MB1901). Inset shows iron speciation data; dotted black lines correspond to highly reactive iron/total iron (Fe_{HR}/Fe_T) values of 0.20 and 0.38 and the dotted red line corresponds to an iron in pyrite/highly reactive iron (Fe_{py}/Fe_{HR}) value of 0.7. **c)** Approximately 1 m of rusty-weathering shale interbedded with basalt (section MB1902). Inset shows iron speciation data. **d)** Turbidite facies (near section MB1613) showing low-angle cross-stratification and soft-sediment deformation.

terpretation of iron speciation data (Raiswell et al., 2018), samples with a Fe_{HR}/Fe_T ratio of >0.38 have experienced authigenic enrichment of highly reactive iron phases that is unique to anoxic environments (samples from modern oxic environments do not have ratios above 0.38; Raiswell and Canfield, 1998). Thus, iron speciation can positively fingerprint anoxic conditions, which is important for understanding how the oxidation of Earth's atmosphere and ocean has changed over time, as well as the concentration of economically important metals in shale. To distinguish between ferruginous (free ferrous iron, no sulphide) and euxinic (free sulphide, iron limited) conditions for anoxic samples, the ratio of iron in pyrite to all highly reactive iron phases (Fe_{py}/Fe_{HR}), including pyrite, is considered. If Fe_{py}/Fe_{HR} is below 0.7, the samples were likely deposited in ferruginous conditions, and if Fe_{py}/Fe_{HR} exceeds 0.7 they were likely deposited in euxinic conditions. Unlike the positive fingerprint for anoxic conditions, however, unambiguous discrimination of oxic conditions is more difficult. Specifically, sediments deposited rapidly, such as in turbidites, are buried before authigenic iron enrichment can occur; modern anoxic turbidite samples reach Fe_{HR}/Fe_T values as low as 0.20 (Sperling et al., 2016). Samples with Fe_{HR}/Fe_T between 0.20 and 0.38 therefore fall into an 'ambiguous' field.

Dark grey and black shales from the Costello Formation have Fe_T values ranging from 1.9 to 9.7 wt. % (mean of 4.9 wt. %); Fe_{HR}/Fe_T ranging from 0.22 to 0.51 (mean of 0.32), with Fe_{py}/Fe_{HR} ranging from 0.00 to 0.53 (mean of 0.12); and TOC ranging from 0.4 to 1.1 wt. % (mean of 0.6 wt. %). Brick-red shales from the Laddie Formation have Fe_T values ranging from 0.2 to 5.8 wt. % (mean of 2.7 wt. %); Fe_{HR}/Fe_T ranging from 0.27 to 1.00 (mean of 0.44), with Fe_{py}/Fe_{HR} ranging from 0.00 to 0.23 (mean of 0.08); and TOC ranging from 0.0 to 0.7 wt. % (mean of 0.1 wt. %). Variably iron-rich argillites from the Kipalu Formation have Fe_T values ranging from 2.8 to 17.5 wt. % (mean of 11.8 wt. %); Fe_{HR}/Fe_T ranging from 0.16 to 0.63 (mean of 0.34) as well as an anomalously high value of 2.57 from the most iron-poor sample, with Fe_{py}/Fe_{HR} consistently 0.00 among all samples. The TOC was not measured in the Kipalu Formation. Dark grey and black shales from the Flaherty Formation have Fe_T values rang-

ing from 3.6 to 9.7 wt. % (mean of 6.2 wt. %); Fe_{HR}/Fe_T ranging from 0.20 to 0.85 (mean of 0.53) as well as an anomalously high value of 1.13 from the most iron-poor sample, with Fe_{py}/Fe_{HR} ranging from 0.06 to 0.83 (mean of 0.34); and TOC ranging from 1.3 to 4.0 wt. % (mean of 2.9 wt. %). Complete geochemical data tables are reported in Hodgskiss and Sperling (2020)[3].

Discussion

The effects of diagenesis, metamorphism and weathering on iron geochemistry

It is important to consider how postdepositional processes may have altered the measured iron speciation values. Increasing metamorphic grades can lead to the transformation of Fe_{carb} to iron in silicate minerals, which would shift Fe_{HR}/Fe_T toward more oxic values (Slotznick et al., 2018a). Regional metamorphism is unlikely to have played a significant role in the transformation of iron minerals (and transfer of iron between the pools considered here) because the Belcher Group underwent prehnite-pumpellyite facies metamorphism (Jackson, 2013). The conversion of pyrite to iron oxides by oxidative weathering is also likely an insignificant factor because rusty weathering was generally minor, and any weathered material was removed during sample preparation.

Samples collected from the Flaherty Formation came from rare shale units approximately 1 m thick in a formation dominated by basalt, and therefore underwent significant thermal metamorphism. This can result in the decomposition of pyrite, leading to loss of sulphur from the sediment, shifting Fe_{py}/Fe_{HR} toward ferruginous values (Yallup et al., 2013; Slotznick et al., 2018a). The formation of pyrrhotite from both pyrite and nonpyrite iron sulphides during contact metamorphism could lead to higher measured Fe_{py}/Fe_{HR} values, because pyrite and pyrrhotite cannot be distinguished by the iron speciation protocol. Alternatively, pyrrhotite could undergo further reactions to form hematite and magnetite, which would shift Fe_{py}/Fe_{HR} toward ferruginous values (Yallup et al., 2013). Finally, Fe_{HR} can react to form iron silicates, which are not extracted during iron speciation, shifting Fe_{HR}/Fe_T values toward oxic values (Slotznick et al., 2018a). The effects of thermal metamorphism, an important factor for interpreting iron speciation results from Flaherty Formation shales, are therefore complex and can shift measurements toward the oxic, ferruginous or euxinic fields.

[3]*CNGO Geoscience Data Series GDS2020-002, containing the data or other information sources used to compile this paper, is available online to download free of charge at http://cngo.ca/summary-of-activities/2019/*

Redox of the Belcher Group

Given that much of the iron speciation data from the Belcher Group fall within the ambiguous field between oxic and anoxic conditions, the geochemical results are difficult to interpret. Nonetheless, an understanding of the redox history of Belcher Group shales can be obtained by integrating sedimentology/basin setting, metamorphic history and outcrop characteristics.

Iron speciation data indicate that deposition of Costello Formation shale took place under ambiguous conditions, with only a small number of samples deposited under unambiguously ferruginous conditions (Figure 8). The Costello Formation is interpreted to have been deposited on the foreslope of the platform, and contains partial Bouma sequences (Ricketts and Donaldson, 1981). Although it is noted that none of these samples are known to record partial Bouma sequences, the influence of distal turbidite deposits cannot be ruled out. The overall turbiditic nature of the succession indicates relatively rapid sedimentation rates (hindering the formation of authigenic iron enrichments), and suggests that the ambiguous iron speciation results can be interpreted as representing ferruginous conditions.

The Laddie Formation was also deposited under intermittently ambiguous to ferruginous conditions, with seven of fifteen samples being unambiguously ferruginous (Figures 8, 9). In contrast to the turbiditic Costello Formation, the Laddie Formation is interpreted as representing sediment-starved, deep-water deposition (Ricketts, 1979). Considering the low sedimentation rate, comparison with modern baselines suggests oxygenated depositional conditions for samples with Fe_{HR}/Fe_T <0.38. One possibility is that these pervasively brick-red, relatively deep-water shales are a marine redbed (MRB). The occurrence of MRBs has been interpreted as reflecting the oxygenation of deep ferruginous waters (Song et al., 2017); local oxygenation of waters during deposition of the Laddie Formation may have been the result of very low rates of organic matter settling. In addition to these iron speciation data, the outcrop appearance of the Laddie Formation bears remarkable similarities with Phanerozoic MRBs (e.g., Song et al., 2017, Figure 1A, B). While the authors by no means suggest pervasive, global oxygenation of the deep ocean during the Orosirian period (2.05–1.8 Ga), both outcrop character and iron speciation data from the Laddie Formation suggest that intermittent oxidation of deep waters could have occurred on a local scale.

Iron speciation data from the Kipalu Formation suggest that deposition took place over a range of conditions, from unambiguously oxic to unambiguously ferruginous (Figure 8), consistent with data reported from other Proterozoic iron formations (e.g., Warchola et al., 2018). The Fe_{py} values in the Kipalu Formation are consistently zero, suggesting that marine sulphate levels were low, as its reduced

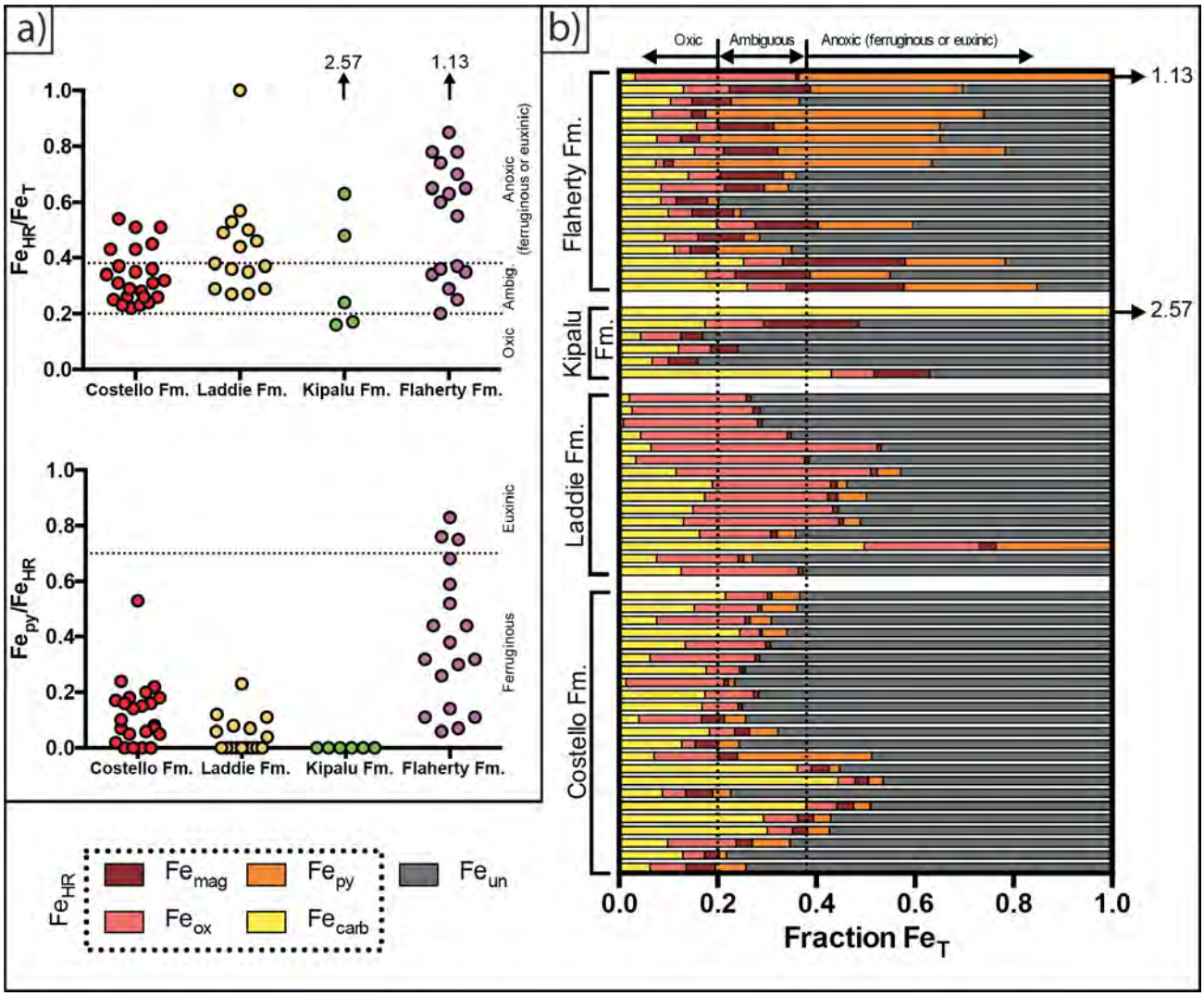

Figure 8: a) Iron speciation data for the Costello (possibly anoxic), Laddie (possibly oxic), Kipalu (oxic to ferruginous) and Flaherty (possibly euxinic) formations, Belcher Group, Belcher Islands. **b)** Individual iron phases plotted as a fraction of total iron. Abbreviations: Fe_{carb}, iron in carbonates; Fe_{HR}, highly reactive iron; Fe_{mag}, iron in magnetite; Fe_{ox}, iron in oxides; Fe_{py}, iron in pyrite; Fe_T, total iron; Fe_{un}, unreactive iron.

form (sulphide) would have reacted with dissolved iron to form iron sulphides.

Finally, the Flaherty Formation records iron speciation values that are indicative of generally ferruginous conditions, with intermittent euxinia (Figure 8). Without more detailed petrographic analyses (e.g., scanning electron microscopy), it is difficult to constrain the effects of contact metamorphism on the iron speciation data, given its ability to make samples appear more oxic (i.e., decrease Fe_{HR}/Fe_T), or alter the balance between ferruginous and euxinic conditions (i.e., change Fe_{py}/Fe_{HR}). The two shale packages in the Flaherty Formation sampled for iron speciation are approximately 1.4 and 1.0 m thick (MB1901 and MB1902, respectively; Figure 7b, c) and are both overlain by pillow basalt, and have thus experienced thermal metamorphism. However, it is noted that both sections have overall trends in which the stratigraphically higher samples (which have undergone more intense contact metamorphism) have lower Fe_{HR}/Fe_T, Fe_{py}/Fe_{HR} and TOC values, suggesting that the most 'primary' iron speciation values reflect euxinia (Figure 7b, c). This is also supported by the highest TOC values within the Belcher Group, up to 4 wt. %. Therefore, it is tentatively interpreted that shales within the Flaherty Formation were deposited within an environment that was at least intermittently euxinic. It is worth noting that these shale units (deposited between 1870 ±3 and 1854.2 ±1.6 Ma; Hamilton et al., 2009; Hodgskiss et al., 2019b) are of very similar age to shale deposited beneath euxinic waters in the Animikie Group, western Lake Superior area, Ontario (between 1878 ±3 and 1836 ±5 Ma; Poulton et al., 2004; Addison et al., 2005). Although both of these successions undoubtedly record some combination of local and global redox signals, the temporal similarities are intriguing.

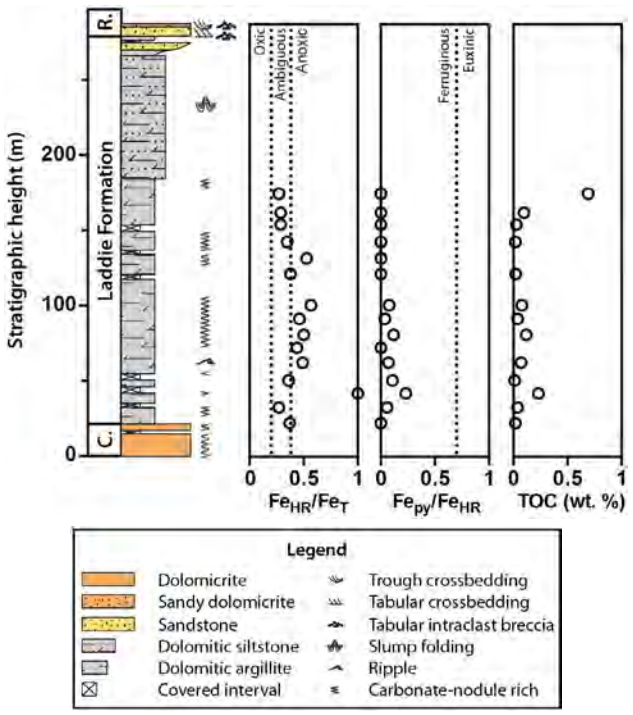

Figure 9: Chemostratigraphic plot of the Laddie Formation, Belcher Islands. Abbreviations: C., Costello Formation; Fe_{HR}, highly reactive iron; Fe_{py}, iron in pyrite; Fe_T, total iron; R., Rowatt Formation.

Redox structure during Belcher Group deposition

Much of the Proterozoic is thought to record low levels of atmospheric oxygen, between 0.1 and 10% of present atmospheric levels (e.g., Cole et al., 2016; Canfield et al., 2018), and it is widely thought that the oxycline (where there is a rapid change in dissolved O_2 concentrations) was very shallow through much of the Proterozoic (e.g., Hardisty et al., 2017). In contrast, the iron speciation data presented here suggest that the oxycline reached the deep basin at least intermittently, and on a local scale, during deposition of the Laddie Formation. Although the anoxic conditions recorded during deposition of the Costello and Flaherty formations are consistent with other successions (e.g., Animikie Group; Poulton et al., 2004), the relatively deep oxic conditions recorded by the Laddie Formation are generally at odds with the anoxic deep waters that are thought to have prevailed through the Proterozoic.

If the Laddie Formation was deposited beneath oxic waters, a likely oceanographic cause for these relatively deep oxic waters is very low surface productivity. The Belcher Group is thought to have been deposited during a time of markedly low gross primary productivity, just 6% of the modern biosphere (Hodgskiss et al., 2019a). This may have allowed for little to no local organic matter loading, in which the oxidation of sinking organic matter drives local redox toward ferruginous or euxinic conditions (e.g., Poulton et al., 2010). This hypothesis is broadly supported by the TOC measurements: the Flaherty Formation, the only formation to record euxinic Fe_{py}/Fe_{HR} values, contains the highest TOC values (mean of 2.9 wt. %), the ferruginous Costello Formation records moderate TOC values (mean of 0.6 wt. %) and the oxic Laddie Formation has the lowest TOC values (mean of 0.1 wt. %).

Economic considerations

Black shales are known to record high concentrations of trace and rare-earth elements, which reach economic concentrations at numerous sites (e.g., Spinks et al., 2016). Many chalcophile and siderophile metals (e.g., molybdenum) are sensitive to redox conditions, and are concentrated in black shales under strongly reducing and especially euxinic conditions (Spinks et al., 2016; Miller et al., 2017). Not only is the occurrence of black shale units extremely limited in the Belcher Group, but they were also generally deposited under oxic or ferruginous conditions, making them poor targets for trace and/or rare-earth elements. Shale interbedded with mafic volcanic rocks in the Flaherty Formation was likely deposited under euxinic conditions, but is volumetrically insignificant. Therefore, the economic potential of shales within the Belcher Group is regarded as extremely low. The Kipalu Formation (with granular iron) has been explored sporadically since the early 1900s (Belcher Mining Corporation Limited, Lundberg Explorations Limited) and most recently in 2011–2012 by Canadian Orebodies Inc. This recent exploration project indicated 230 million tonnes of iron ore at 35.15% iron, although no development seems to have occurred since 2012, when significant concerns were raised by local land users.

Conclusions

The iron speciation data presented here, the first for the Belcher Group, suggest that deposition of shale units took place largely within ferruginous to weakly oxic waters. Notably, the Laddie Formation appears to record oxic waters even in the deep basin, and may constitute a Paleoproterozoic marine redbed, which do not become volumetrically significant until almost 1500 m.y. later. These data suggest a surprisingly deep oxycline during the Orosirian period, at least at some points locally within the Belcher Group. Shale units deposited within the Flaherty Formation have undergone intense contact metamorphism, but likely record deposition beneath euxinic waters that may be coincident with the development of euxinic conditions in the Animikie Basin, ~1200 km to the southwest. Overall, these data provide a new perspective on the evolution of Earth's oceans as recorded in the Belcher Group and through the Orosirian period.

Acknowledgments

The authors thank R.H. Rainbird for thoughtful and detailed comments on this manuscript. The support of the citi-

zens of Sanikiluaq, the Sanikiluaq Hamlet Office and the Sanikiluaq Hunters and Trappers Association is greatly appreciated. The authors especially thank J. Iqaluk, G. and A. Rumbolt, L. and P. Ippak, J. Inuktaluk and T. Appaqaq for their professional and reliable guiding through the Belcher Islands. J.L. Frost (2016), O.M.J. Dagnaud (2017) and B.S. McDonald and Z.A. Pollock (2019) are thanked for their assistance during this fieldwork. Helpful discussions highlighting the nuances of diagenesis and metamorphism on the iron speciation proxy were provided by N.L. Swanson-Hysell and S.P. Slotznick. Finally, T.N. Browne is thanked for assistance conducting iron speciation and total organic carbon measurements. This project was supported by the Postgraduate Scholarships-Doctoral program of the Natural Sciences and Engineering Research Council of Canada, and by student research grants from National Geographic, the American Philosophical Society Lewis and Clark Fund, Northern Scientific Training Program, McGill University Graduate Research Enhancement and Travel (GREAT) awards program, Geological Society of America, Mineralogical Association of Canada and Stanford University's McGee Fund and Bob Compton Fund.

References

Addison, W.D., Brumpton, G.R., Vallini, D.A., McNaughton, N.J., Davis, D.W., Kissin, S.A., Fralick, P.W. and Hammond, A.L. 2005: Discovery of distal ejecta from the 1850 Ma Sudbury impact event; Geology, v. 33, p. 193–196, URL <https://doi.org/10.1130/G21048.1>.

Baragar W.R.A. and Scoates, R.F.J. 1981: The Circum-Superior belt: a Proterozoic plate margin?; Developments in Precambrian Geology, v. 4, p. 297–330, URL <https://doi.org/10.1016/S0166-2635(08)70017-3>.

Bell, R.T. and Jackson, G.D. 1974: Aphebian halite and sulphate indications in the Belcher Group, Northwest Territories; Canadian Journal of Earth Sciences, v. 11, p. 722–728, URL <https://doi.org/10.1139/e74-072>.

Canfield, D.E., Raiswell, R., Westrich, J.T., Reaves, C.M. and Berner, R.A. 1986: The use of chromium reduction in the analysis of reduced inorganic sulfur in sediments and shales; Chemical Geology, v. 54, p. 149–155, URL <https://doi.org/10.1016/0009-2541(86)90078-1>.

Canfield, D.E., Zhang, S., Frank, A.B., Wang, X., Wang, H., Su, J., Ye, Y. and Frei, R. 2018: Highly fractionated chromium isotopes in Mesoproterozoic-aged shales and atmospheric oxygen; Nature Communications, v. 9, p. 11, URL <https://doi.org/10.1038/s41467-018-05263-9>.

Cole, D.B., Reinhard, C.T., Wang, X., Gueguen, B., Halverson, G.P., Gibson, T., Hodgskiss, M.S.W., McKenzie, N.R., Lyons, T.W. and Planavsky, N.J. 2016: A shale-hosted Cr isotope record of low atmospheric oxygen during the Proterozoic; Geology, v. 44, p. 555–558, URL <https://doi.org/10.1130/G37787.1>.

Dimroth, E., Baragar, W.R.A., Bergeron, R. and Jackson, G.D. 1970: The filling of the Circum-Ungava geosyncline; *in* Basins and Geosynclines of the Canadian Shield, A.J. Baer (ed.), Geological Survey of Canada, Paper 70-40, p. 45–142.

Hamilton, M., Buchan, K., Ernst, R. and Stott, G. 2009: Widespread and short-lived 1870 Ma mafic magmatism along the northern Superior craton margin; American Geophysical Union – Geological Association of Canada Joint Meeting, Abstract # GA11A-01.

Hardisty, D.S., Lu, Z., Bekker, A., Diamond, C.W., Gill, B.C., Jiang, G., Kah, L.C., Knoll, A.H., Loyd, S.J., Osburn, M.R., Planavsky, N.J., Wang, C., Zhou, X. and Lyons, T.W. 2017: Perspectives on Proterozoic surface ocean redox from iodine contents in ancient and recent carbonate; Earth and Planetary Science Letters, v. 463, p. 159–170, URL <https://doi.org/10.1016/j.epsl.2017.01.032>.

Hodgskiss, M.S.W. and Sperling, E.A. 2020: Data table accompanying "Stratigraphy and shale geochemistry of the Belcher Group, Belcher Islands, southern Nunavut"; Canada-Nunavut Geoscience Office, Geoscience Data Series GDS2020-002, Microsoft® Excel® file, URL <http://cngo.ca/summary-of-activities/2019/>.

Hodgskiss, M.S.W., Crockford, P.W., Peng, Y., Wing, B.A. and Horner, T.J. 2019a: A productivity collapse to end Earth's Great Oxidation; Proceedings of the National Academy of Sciences of the United States of America, v. 116, p. 17207–17212, URL <https://doi.org/10.1073/pnas.1900325116>.

Hodgskiss, M.S.W., Dagnaud, O.M.J., Frost, J.L., Halverson, G.P., Schmitz, M.D., Swanson-Hysell, N.L. and Sperling E.A. 2019b: New insights on the Orosirian carbon cycle, early Cyanobacteria, and the assembly of Laurentia from the Paleoproterozoic Belcher Group; Earth and Planetary Science Letters, v. 520, p. 141–152, URL <https://doi.org/10.1016/j.epsl.2019.05.023>.

Hofmann, H.J. 1976: Precambrian microflora, Belcher Islands, Canada: significance and systematics; Journal of Paleontology, v. 50, p. 1040–1073.

Hofmann, H.J. and Jackson, G.D. 1987: Proterozoic ministromatolites with radial-fibrous fabric; Sedimentology, v. 34, p. 963–971, URL <https://doi.org/10.1111/j.1365-3091.1987.tb00586.x>.

Jackson, G.D. 1960: Belcher Islands, Northwest Territories, 33M, 34D, E; Geological Survey of Canada, Paper 60-20, 13 p.

Jackson, G.D. 1961: Geology, Belcher Islands, District of Keewatin, Northwest Territories; Geological Survey of Canada, Preliminary Map 28-1960, scale 1:126 720.

Jackson, G.D. 2013: Geology, Belcher Islands, Nunavut; Geological Survey of Canada, Open File 4923, 159 p., URL <https://doi.org/10.4095/292434>.

Miller, A.J., Strauss, J.V., Halverson, G.P., Macdonald, F.A., Johnston, D.T. and Sperling, E.A. 2017: Tracking the onset of Phanerozoic-style redox-sensitive trace metal enrichments: new results from basal Ediacaran post-glacial strata in NW Canada; Chemical Geology, v. 457, p. 24–37, URL <https://doi.org/10.1016/j.chemgeo.2017.03.010>.

Moore, E.S. 1918: The iron-formation on Belcher Islands, Hudson Bay, with special reference to its origin and its associated algal limestones; Journal of Geology, v. 26, p. 412–438.

Poulton, S.W. and Canfield, D.E. 2005: Development of a sequential extraction procedure for iron: implications for iron partitioning in continentally derived particulates; Chemical Geology, v. 214, p. 209–221, URL <https://doi.org/10.1016/j.chemgeo.2004.09.003>.

Poulton, S.W., Fralick, P.W. and Canfield, D.E. 2004: The transition to a sulphidic ocean ~1.84 billion years ago; Nature, v. 431, p. 173–177, URL <https://doi.org/10.1038/nature02912>.

Poulton, S.W., Fralick, P.W. and Canfield, D.E. 2010: Spatial variability in oceanic redox structure 1.8 billion years ago; Nature Geoscience, v. 3, p. 486–490, URL <https://doi.org/10.1038/ngeo889>.

Raiswell, R. and Canfield, D.E. 1998: Sources of iron for pyrite formation in marine sediments; American Journal of Science, v. 298, no. 3, p. 219–245, URL <https://doi.org/10.2475/ajs.298.3.219>.

Raiswell, R., Hardsity, D.S., Lyons, T.W., Canfield, D.E., Owens, J.D., Planavsky, N.J., Poulton, S.W. and Reinhard, C.T. 2018: The iron paleoredox proxies: a guide to the pitfalls, problems, and proper practice; American Journal of Science, v. 318, p. 491–526, URL <https://doi.org/10.2475/05.2018.03>.

Rasmussen, B., Fletcher, I.R., Bekker, A., Muhling, J.R., Gregory, C.J. and Thorne, A.M. 2012: Deposition of 1.88-billion-year-old iron formations as a consequence of rapid crustal growth; Nature, v. 484, p. 498–501, URL <https://doi.org/10.1038/nature11021>.

Ricketts, B.D. 1979: Sedimentology and stratigraphy of eastern and central Belcher Islands, Northwest Territories; Ph.D. thesis, Carleton University, Ottawa, Ontario, 314 p.

Ricketts, B.D. and Donaldson, J.A. 1981: Sedimentary history of the Belcher Group of Hudson Bay; *in* Proterozoic Basins of Canada, F.H.A. Campbell (ed.), Geological Survey of Canada, Paper 81-10, p. 235–254.

Ricketts, B.D. and Donaldson, J.A. 1988: Stromatolite reef development on a mud-dominated platform in the middle Precambrian Belcher Group of Hudson Bay; *in* Reefs, Canada and Adjacent Area, H.H.J. Geldsetzer, N.P. James and G.E. Tebbutt (ed.), Canadian Society of Petroleum Geologists, Memoir 13, p. 113–119.

Slotznick, S.P., Eiler, J.M. and Fischer, W.W. 2018a: The effects of metamorphism on iron mineralogy and the iron speciation redox proxy; Geochimica et Cosmochimica Acta, v. 224, p. 96–115, URL <https://doi.org/10.1016/j.gca.2017.12.003>.

Slotznick, S.P., Swanson-Hysell, N.L. and Sperling, E.A. 2018b: Oxygenated Mesoproterozoic lake revealed through magnetic mineralogy; Proceedings of the National Academy of Science of the United States of America, v. 115, p. 12938–12943, URL <https://doi.org/10.1073/pnas.1813493115>.

Song, H., Jiang, G., Poulton, S.W., Wignall, P.B., Tong, J., Song, H., An, Z., Chu, D., Tian, L., She, Z. and Wang, C. 2017: The onset of widespread marine red beds and the evolution of ferruginous oceans; Nature Communications, v. 8, p. 7, URL <https://doi.org/10.1038/s41467-017-00502-x>.

Sperling, E.A., Carbone, C., Strauss, J.V., Johnston, D.T., Narbonne, G.M. and Macdonald, F.A. 2016: Oxygen, facies, and secular controls on the appearance of Cryogenian and Ediacaran body and trace fossils in the Mackenzie Mountains of northwestern Canada; Geological Society of America Bulletin, v. 128, p. 558–575, URL <https://doi.org/10.1130/B31329.1>.

Spinks, S.C., Schmid, S., Pagéa, A. and Bluett, J. 2016: Evidence for SEDEX-style mineralization in the 1.7 Ga Tawallah Group, McArthur Basin, Australia; Ore Geology Reviews, v. 76, p. 122–139, URL <https://doi.org/10.1016/j.oregeorev.2016.01.007>.

Stookey, L.L. 1970: Ferrozine – a new spectrophotometric reagent for iron; Analytical Chemistry, v. 42, p. 779–781, URL <https://doi.org/10.1021/ac60289a016>.

Warchola, T., Lalonde, S.V., Pecoits, E., von Gunten, K., Robbins, L.J., Alessi, D.S., Philippot, P. and Konhauser, K.O. 2018: Petrology and geochemistry of the Boolgeeda Iron Formation, Hamersley Basin, Western Australia; Precambrian Research, v. 316, p. 155–173, URL <https://doi.org/10.1016/j.precamres.2018.07.015>.

Yallup, C., Edmonds, M. and Turchyn, A.V. 2013: Sulfur degassing due to contact metamorphism during flood basalt eruption; Geochimica et Cosmochimica Acta, v. 120, p. 263–279, URL <https://doi.org/10.1016/j.gca.2013.06.025>.